Nucleic Acids Research, 2005, Vol. 33, No. 12 ***3919–3931***
doi:10.1093/nar/gki694

Kinetics of substrate recognition and cleavage by human 8-oxoguanine-DNA glycosylase

Nikita A. Kuznetsov[1,2], Vladimir V. Koval[1,2], Dmitry O. Zharkov[1,2], Georgy A. Nevinsky[1,2], Kenneth T. Douglas[3] and Olga S. Fedorova[1,2,*]

[1]Institute of Chemical Biology and Fundamental Medicine, Siberian Branch of the Russian Academy of Sciences, Novosibirsk 630090, Russia, [2]Novosibirsk State University, Novosibirsk 630090, Russia and [3]School of Pharmacy and Pharmaceutical Sciences, University of Manchester, Manchester M13 9PL, UK

Received February 3, 2005; Revised May 4, 2005; Accepted June 16, 2005

ABSTRACT

Human 8-oxoguanine-DNA glycosylase (hOgg1) excises 8-oxo-7,8-dihydroguanine (8-oxoG) from damaged DNA. We report a pre-steady-state kinetic analysis of hOgg1 mechanism using stopped-flow and enzyme fluorescence monitoring. The kinetic scheme for hOgg1 processing an 8-oxoG:C-containing substrate was found to include at least three fast equilibrium steps followed by two slow, irreversible steps and another equilibrium step. The second irreversible step was rate-limiting overall. By comparing data from Ogg1 intrinsic fluorescence traces and from accumulation of products of different types, the irreversible steps were attributed to two main chemical steps of the Ogg1-catalyzed reaction: cleavage of the *N*-glycosidic bond of the damaged nucleotide and β-elimination of its 3′-phosphate. The fast equilibrium steps were attributed to enzyme conformational changes during the recognition of 8-oxoG, and the final equilibrium, to binding of the reaction product by the enzyme. hOgg1 interacted with a substrate containing an aldehydic AP site very slowly, but the addition of 8-bromoguanine (8-BrG) greatly accelerated the reaction, which was best described by two initial equilibrium steps followed by one irreversible chemical step and a final product release equilibrium step. The irreversible step may correspond to β-elimination since it is the very step facilitated by 8-BrG.

INTRODUCTION

Oxidative stress, both of environmental and metabolic origin, presents an ongoing challenge for cellular DNA (1). Nucleobases and deoxyribose are both prone to oxidation, which generates a number of different lesions (2–4). The most common purine base redox lesions *in vivo* are 8-oxoguanine (8-oxoG) (Figure 1), 8-oxoadenine, 4,5-diamino-5-formamidopyrimidine (FapyAde) (derived from adenine) and 2,6-diamino-4-hydroxy-5-formamidopyrimidine (FapyGua) (derived from guanine) (5). Incorporation of inappropriate nucleotides by DNA polymerases opposite these lesions results in their considerable mutagenicity (6–9). To counteract this damage, many organisms possess a three-component enzymatic system (termed 'GO system' after 8-oxoG), shown to reduce mutagenesis by 8-oxoG (10,11) and possibly by other oxidized purines. The GO system of *Escherichia coli* consists of three enzymes, 8-oxodGTPase (MutT), mismatched adenine DNA glycosylase (MutY) and 8-oxoG-DNA glycosylase (Fpg or MutM). MutT prevents incorporation of 8-oxoG to DNA from the pool of oxidized dGTP, Fpg removes 8-oxoG from 8-oxoG:C pairs, and MutY removes adenine from A:8-oxoG pairs, which could only arise in DNA after a misincorporation event (10,11). A fully functional GO system decreases the rate of spontaneous mutagenesis 250-fold in *E.coli* (12).

Most eukaryotes have homologues of MutT (13) and MutY (14). However, the major eukaryotic 8-oxoG-DNA glycosylase, Ogg1, is not homologous to bacterial Fpg (15,16). Ogg1 belongs to a superfamily of endonuclease III-like DNA glycosylases possessing conserved structural helix–hairpin–helix and G/P . . . D-loop motifs (17,18), whereas Fpg is a prototypic member of another DNA repair enzyme superfamily characterized by the presence of a helix–two turn–helix motif and a Cys_4 zinc finger (19,20). Because of these structural differences, Ogg1 and Fpg also differ in the nature of nucleophiles used to initiate base excision (21,22) in the type of the break left in DNA after base excision (15) and in steady-state reaction kinetics (23,24). In addition, the substrate specificities of these two enzymes overlap only partially (23–27), the main difference being that FapyAde is not a

*To whom correspondence should be addressed. Tel: +7 383 330 92 74; Fax: +7 383 333 36 77; Email: fedorova@nibosch.nsc.ru

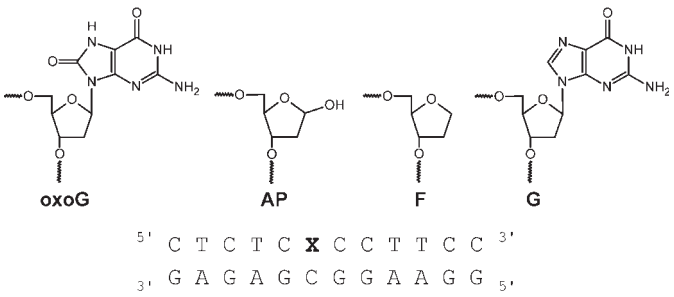

Figure 1. Chemical nature of the lesions used in this study and the sequences of oligonucleotides used.

substrate for Ogg1. However, enzymes homologous and structurally similar to Fpg (e.g. endonuclease VIII) or Ogg1 (e.g. endonuclease III) can have quite different substrate specificities despite all the similarities (28).

Ogg1 is a bifunctional enzyme, possessing DNA glycosylase activity (hydrolysis of the *N*-glycosidic bond of the damaged nucleotide) and AP lyase activity (elimination of the 3′-phosphate, often referred to as β-elimination). Unlike the situation in several other bifunctional DNA glycosylases, the AP lyase activity of Ogg1 is much weaker than its glycosylase activity (24,29). Consequently, two products of Ogg1-catalyzed reaction can be detected: the glycosylase activity quickly produces abasic (AP) sites, and a slower AP lyase activity leaves nicked DNA with the nick flanked by a 5′-phosphate and a 3′-terminal α,β-unsaturated aldehyde. If Ogg1 is presented with an AP site-containing substrate, the rate of its cleavage is similar to the rate of β-elimination of a damaged base-containing substrate (24). This rate can be significantly elevated if the reaction mixture contains guanine derivatives substituted with an electron-withdrawing group at C8, such as 8-bromoguanine (8-BrG), which probably acts as a cofactor promoting dissociation of a proton at C2′ (30).

It is being increasingly realized that the substrate specificity of DNA- or RNA-dependent enzymes depends not only on the structural features of the Michaelis complex, but also on the other points along the reaction coordinate (31–34). Whether a given lesion will be recognized and excised by a DNA glycosylase may depend on the series of conformational changes in both the enzyme and DNA molecule that start at the moment of the enzyme binding to unspecific DNA and bring the reacting moieties to positions permitting the act of catalysis; different steps of the reaction coordinate may be 'bottlenecks' at which non-substrates are discriminated against (31,33–35).

Recently, pre-steady-state kinetic analysis of *E.coli* Fpg acting on undamaged DNA, 8-oxoG, a natural AP site and an uncleavable tetrahydrofuran analogue of an AP site (F) has been reported (36,37). To address the question whether a structurally different enzyme uses similar or different mechanisms in recognizing and processing the same lesion, we now extend this analysis to human Ogg1 using the same set of substrates. The results reported here suggest that, although Ogg1 uses a generally quite different kinetic scheme to recognize and excise 8-oxoG, some steps are remarkably similar between Ogg1 and Fpg, supporting the idea that lesion recognition strongly depends on its nature. In addition, we investigate the kinetic mechanism of stimulation of AP lyase activity of Ogg1 by 8-BrG and show that the stimulation results from an increase in the rate of β-elimination.

MATERIALS AND METHODS

Materials, oligonucleotides, enzymes and bacterial strains

Chemicals were mostly from Sigma–Aldrich (St Louis, MO). 8-BrG was synthesized according to a published procedure (38). Oligodeoxyribonucleotides for stopped-flow experiments (Figure 1) were prepared as described previously (36,37). PCR primers were made by Sigma–Genosys (Woodlands, TX), purified by 20% PAGE and desalted using SepPak reverse-phase cartridge (Waters, Milford, MA). Vector pET-15b DNA and *E.coli* BL21(DE3) cells were from Novagen (Madison, WI). Restriction endonuclease XhoI, T4 polynucleotide kinase and T4 DNA ligase were from New England Biolabs (Beverly, MA); restriction endonuclease Bpu1102I and *Pfu* DNA polymerase were from Stratagene (La Jolla, CA). [γ-^{32}P]ATP (>3000 Ci/mmol) was from Biosan (Novosibirsk, Russia).

Cloning of hOgg1 for overexpression

To make a construct for overexpression of the main hOgg1 isoform, hOgg1-1a, its full-length coding sequence was PCR-amplified from human testis QUICK-Clone cDNA (Clontech, Palo Alto, CA) using the primers d(CGAGACCTCGAGCCTGCCCGCGCGCTTCTGCC) (carries a XhoI restriction site) and d(CGAGACGCTCAGCCTAGCCTTCCGGCCCTTTGG) (carries a Bpu1102I restriction site). Thirty cycles of PCR (1 min at 94°C, 1 min at 60°C and 2 min at 72°C) were performed with *Pfu* DNA polymerase according to the manufacturer's instructions. Of the two bands visible after resolution of the products by electrophoresis in 1% agarose gel, one (1 kb long) is expected to correspond to the 1a isoform of hOgg1, and the other (1.3 kb long) to the 1b isoform. The 1 kb fragment was extracted using the QIAquick gel extraction kit (Qiagen, Valencia, CA), digested with Bpu1102I and XhoI, purified by MiniElute PCR purification (Qiagen) and ligated into pET-15b vector digested with the same enzymes. Ligation products were electroporated into *E.coli* DH5α cells using an *E.coli* Pulser (Bio-Rad, Hercules, CA) following the manufacturer's protocol. The sequence of the insert, confirmed by direct sequencing, was found to be identical to the published data (16). The construct, termed phOgg11aNHis, expresses a full-length hOgg1-1a protein tagged at the N-terminus with a hexahistidine oligopeptide followed by a linker of 13 amino acid residues. The protein terminates at the native C-terminus of hOgg1-1a.

Purification of hOgg1

To purify hOgg1 expressed as a recombinant protein in *E.coli*, 2 litres of *E.coli* BL21(DE3) carrying the phOgg11aNHis construct were grown in YT×2 broth with 50 μg/ml ampicillin at 37°C until A_{600} = 0.6–0.7, then shifted to 30°C and induced overnight with 0.2 mM isopropyl-β-D-thiogalactopyranoside. The cells were harvested by centrifugation, resuspended in lysis buffer (40 ml of 100 mM Tris–HCl, pH 8.0, 1 mM EDTA) supplemented with 1 mM phenylmethylsulfonyl fluoride and incubated with lysozyme (0.5 mg/ml) for 30 min at room temperature. Incubation was continued for a further 30 min after the addition of NaCl to 1 M. Lysis was then completed by

sonicating the suspension on ice using an UZDN-2T ultrasound dispergator (SELMI, Ukraine), with 10 pulses of 30 s at the highest power setting, with a 90 s interval between pulses. The lysate was clarified by centrifugation (12 000 *g*, 4°C, 30 min) and diluted with 4 vol of Buffer A (25 mM potassium phosphate, pH 7.4). The resulting solution was applied to a column of Fractogel EMD SO_3^- 650 (Merck, 50 ml packed bed volume) equilibrated in Buffer A with 200 mM NaCl. The column was washed with 120 ml of the equilibration buffer. Then, the column outlet was connected to a 5 ml HiTrap Chelating column (Pharmacia) charged with Ni^{2+}, and the whole system was washed with Buffer A containing 1 M NaCl. The chelating column was then disconnected, washed with Buffer A containing 500 mM NaCl and 50 mM imidazole, and the hexahistidine-tagged polypeptides were eluted in Buffer A with 500 mM NaCl and 500 mM imidazole. The eluate was diluted 10-fold with Buffer A and applied to a 5 ml HiTrap heparin column (Pharmacia) equilibrated in Buffer A with 200 mM NaCl. The column was developed with a gradient of 200–800 mM NaCl in Buffer A; the fractions absorbing at 280 nm were collected, supplemented with DTT to 1 mM and analyzed by 12% discontinuous gel electrophoresis (Laemmli system). Fractions containing a band of the expected mobility (typically ~20 ml) were pooled, dialyzed against two changes of 250 ml of 25 mM potassium phosphate, pH 7.4, 400 mM NaCl, 1 mM EDTA, 1 mM DTT, 50% glycerol and stored at −20°C. The enzyme was electrophoretically homogeneous.

Stopped-flow experiments

The experiments were conducted and numerical values for kinetic constants extracted as described previously for Fpg protein (37), except that fluorescent traces were obtained for times up to 1000 s. All experiments were carried out at 25°C in a buffer containing 50 mM Tris–HCl, pH 7.5, 50 mM KCl, 1 mM EDTA, 1 mM DDT and 9% glycerol (v/v). A model SX.18MV stopped-flow spectrometer (Applied Photophysics Ltd, Leatherhead, UK) fitted with a 150 W Xe arc lamp and 2 mm pathlength optical cell was used with excitation at 283 nm. Fluorescence emission from enzyme Trp residues was observed through a 320 nm long-pass filter. The dead time of the instrument was 1.4 ms. Only data at times >2 ms were used for calculation. hOgg1 in one syringe was rapidly mixed with a solution of the substrate in the other syringe. The concentration of hOgg1 in the reaction chamber after mixing in all experiments was 1.0 μM, and concentrations of ODN substrates were varied in the range 0.25–3.0 μM. Typically, each trace shown is the average of four or more individual experiments; reported rate constants represent the mean (with standard deviation) of such datasets.

Bleaching of enzyme fluorescence

When a solution of hOgg1 was mixed with buffer, fluorescence bleaching was observed. For the correction of the measured data, the fluorescence intensities were recalculated using Equation 1:

$$F = (F_{obs} - F_b) \times \exp(k_b \times t) + F_b \quad \mathbf{1}$$

where F is the corrected fluorescence intensity, F_{obs} is the observed fluorescence intensity, F_b is the background fluorescence, and k_b is the coefficient determined for each substrate concentration in experiments with non-cleaved substrates.

Inner filter effect

F-values in the presence of ODN substrates were also corrected for the inner filter effect due to ODN absorption at 293 nm using the following equation:

$$F_c = F \times 10^{0.5 \times A_{ex}} \quad \mathbf{2}$$

where F_c is the fluorescence intensity at the particular wavelength, corrected both for bleaching and the inner filter effect, and A_{ex} is the absorbance of the ODNs at 293 nm.

Kinetic data analysis

Global non-linear least-squares fitting was performed using DynaFit software (BioKin Ltd) (39). Differential equations were written for each species in the mechanisms described in Schemes 1–4 (see Results), and the stopped-flow fluorescence traces were directly fit by expressing the corrected fluorescence intensity (F_c) at any reaction time t as the sum of the background fluorescence (F_b) and the fluorescence intensities of each protein species:

$$F_c = F_b + \sum_{i=0}^{n} F_i(t) \quad \mathbf{3}$$

where $F_i(t) = f_i(E_i(t))$, f_i are the coefficients of specific fluorescence for each discernible hOgg1 conformer, and ($E_i(t)$) are the concentrations of the conformers at any given time t ($i = 0$ relates to the free protein; $i > 0$ relates to the protein–DNA complexes) These specific fluorescence coefficients describe only the part of fluorescence that changes due to DNA binding.

Fluorescence titration of hOgg1 with oligonucleotide ligands under stationary conditions

Each point on the fluorescence titration curves was obtained by measurement of the fluorescence intensity of separate solutions (80 μl) containing hOgg1 (1×10^{-6} M) and oligonucleotide ligand at the required concentration in a binding buffer (50 mM Tris–HCl, pH 7.5, 50 mM KCl, 1 mM EDTA, 1 mM DTT and 9% glycerol). The mixtures were incubated at 25°C for 2 min. Fluorescence spectra were measured at the excitation wavelength of 283 nm using an SFM 25 spectrofluorometer (Kontron Instruments, Italy) in minimum time possible to avoid bleaching. Values of fluorescence intensity at the emission maximum (333 nm) were used to calculate the association constants according to the equations:

$$K_d = \frac{[\text{ligand}][\text{hOgg1}]}{[\text{complex}]} \quad \mathbf{4}$$

The mass-balance equations are written as:

$$[\text{ligand}]_0 = [\text{ligand}] + [\text{complex}] \quad \mathbf{5}$$

$$[\text{hOgg1}]_0 = [\text{hOgg1}] + [\text{complex}] \quad \mathbf{6}$$

where $[\text{ligand}]_0$ and $[\text{hOgg1}]_0$ are the total amounts of the oligonucleotide ligand and hOgg1, respectively; [ligand], [hOgg1] and [complex] are the concentrations of the free ligand, hOgg1 and their complex, respectively.

The intensity of the detected fluorescence F can be expressed as:

$$F = f_{\text{hOgg1}} \times [\text{hOgg1}] + f_{\text{complex}} \times [\text{complex}] \quad \mathbf{7}$$

$$f_{\text{hOgg1}} = F_0/[\text{hOgg1}]_0;\ f_{\text{complex}} = F_{\text{lim}}/[\text{hOgg1}]_0 \quad \mathbf{8}$$

where F_0, F_{lim} are the fluorescence intensities at [ligand] = 0 and at very high concentration of ligand (at the end of curve), respectively; f_{hOgg1} and f_{complex} are the partial fluorescence intensities of free hOgg1 and its complex.

It follows from Equations 4 to 6 that the concentration of free hOgg1 is described by Equation 9:

$$[\text{hOgg1}] = \frac{[\text{hOgg1}]_0 - [\text{ligand}]_0 - K_d}{2} + \sqrt{\left(\frac{[\text{hOgg1}]_0 - [\text{ligand}]_0 - K_d}{2}\right)^2 + K_d[\text{hOgg1}]_0} \quad \mathbf{9}$$

Combining Equations 4–7 and 9 results in Equation 10, describing the ratio between observed fluorescence intensity F and K_d:

$$F = f_{\text{complex}}[\text{hOgg1}]_0 + (f_{\text{hOgg1}} - f_{\text{complex}}) \times \left\{\frac{[\text{hOgg1}]_0 - [\text{ligand}]_0 - K_d}{2} + \sqrt{\left(\frac{[\text{hOgg1}]_0 - [\text{ligand}]_0 - K_d}{2}\right)^2 + K_d[\text{hOgg1}]_0}\right\} \quad \mathbf{10}$$

Product analysis

To analyze products formed by Ogg1, the substrate oligonucleotides were 5′-^{32}P-labeled using T4 polynucleotide kinase and [γ-^{32}P]ATP, and the reaction was performed under the conditions described above. The products were precipitated by adding 10 vol of 2% $LiClO_4$/acetone solution. The precipitates were washed three times with 100 µl of acetone, dried, dissolved in water (4 µl) and formamide dye loading buffer (3 µl), and analyzed by 20% denaturing PAGE. The gels exposed on Agfa CP-BU X-ray film (Agfa-Geavert, Belgium), and the autoradiograms were scanned and quantified using Gel-Pro Analyzer software (Media Cybernetics, USA).

Structural analysis

To analyze the movement of Trp residues between two adjacent Ogg1 structures, protein parts of the structures were superimposed for the best fit of their backbones, and the root-mean-square deviation (r.m.s.d.) was calculated for the side chains of the individual Trp residues using Swiss-PdbViewer v3.7 (40). Water-accessible surfaces of individual Trp residues were calculated using GETAREA 1.1 (41).

RESULTS

Ogg1 fluorescence changes due to substrate binding

Time-dependent stopped-flow experiments were carried out using dodecamer duplex substrates containing a single lesion at the sixth position from the 5′ end of the modified strand (Figure 1). Such duplexes are stable under the conditions used (36,37). The footprint of Ogg1, as judged from its crystal structure in a complex with DNA, does not exceed 9–10 bp (30,42,43). The terminal effects on Ogg1 kinetics are negligible when the lesion is located 5 bp away from any terminus (D. O. Zharkov, unpublished data). Fluorescence spectra of Ogg1 in the absence and presence of non-specific duplex were measured under equilibrium conditions. Binding to the duplex caused a change in the enzyme fluorescence (data not shown), confirming that direct internal tryptophan fluorescence could be used to monitor the reaction progress in stopped-flow experiments.

Binding of Ogg1 to DNA duplexes containing G:C, F:C and AP:C

To obtain a reference base for the analysis of Ogg1 interactions with substrates containing lesions, we first investigated binding of Ogg1 to an undamaged dsODN of the same sequence. As shown in Figure 2, the intrinsic Trp fluorescence of Ogg1 showed a slow decrease over a 10 s time range. The fluorescence traces for G:C and F:C duplexes showed rather low signal-to-noise ratio, making their quantitative processing not very reliable. Fitting the data for AP:C to the one-site binding model (36) gave estimates for the forward and reverse rate constants of Ogg1 binding to an AP:C substrate of 4.6×10^5 M^{-1} s^{-1} and 0.11 s^{-1}, respectively, corresponding to an equilibrium dissociation constant $K_{\text{ESf}} = 2.4 \times 10^{-7}$ M. (Throughout the paper, rate or equilibrium constants determined in the stopped-flow experiments are denoted by subscript index 'f', those determined in fluorescence titration experiments, by subscript index 't', and the constants determined in electrophoresis experiments, by subscript index 'e'. Substrates for which the constants were determined are shown as superscript indexes, if necessary.)

For the AP:C ligand, such a result was rather unexpected, since Ogg1 has been reported to process such substrates by β-elimination, albeit not very efficiently (24,29). Nevertheless, it is evident from Figure 2 that though there is no significant

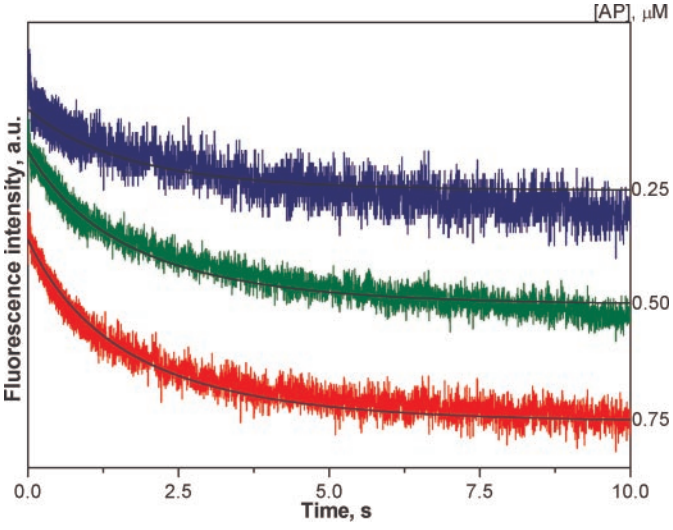

Figure 2. Fluorescence traces for binding of hOgg1 to AP:C ligand. Colored traces represent experimental data; black curves are theoretically fitted.

processing of the AP:C substrate, the enzyme binds natural AP sites tightly enough.

Interaction of Ogg1 with 8-oxoG:C-containing duplexes

In contrast to the three dsODN ligands described above, the duplex containing an 8-oxoG:C pair showed more complex fluorescence dynamics (Figure 3A). At least five discernible fluorescence change steps could be observed in the fluorescence traces. The reaction rate of mammalian Ogg1 is known to be limited by the product release step (24,44), and the rate of the Ogg1-catalyzed AP lyase reaction is notably lower than that of the glycosylase reaction (24). Accordingly, processing of the 8-oxoG:C-containing substrate by Ogg1 was described in Scheme 1.

$$E + S \underset{k_{1r}}{\overset{k_{1f}}{\rightleftharpoons}} ES1 \underset{k_{2r}}{\overset{k_{2f}}{\rightleftharpoons}} ES2 \underset{k_{3r}}{\overset{k_{3f}}{\rightleftharpoons}} ES3 \xrightarrow{k_{4f}} EP \xrightarrow{k_{5f}} E + P$$

Scheme 1. Binding and cleavage of an 8-oxoG:C-containing substrate by Ogg1. (ES)i, different enzyme-substrate complexes.

The values for individual kinetic constants were determined by global fitting (Table 1). Equilibrium constants for the first three steps, as well as the overall association constant, can be calculated from these data as $K_{1f} = 2.0 \times 10^6$ M^{-1}, $K_{2f} = 11.5$ M^{-1} and $K_{3f} = 0.17$ M^{-1} (overall $K_{Af} = 2.9 \times 10^7$ M^{-1}).

The slow rate of enzyme turnover did not allow us to analyze reliably the advanced stages of the reaction. Given the

Table 1. Rate constants for interactions of Ogg1 with 8-oxoG:C

Rate constant	Mean ± SD
$k_{1f}^{(oG:C)}$ (M^{-1} s^{-1})	$(2.6 \pm 0.1) \times 10^8$
$K_{-1f}^{(oG:C)}$ (s^{-1})	130 ± 1
$k_{2f}^{(oG:C)}$ (s^{-1})	13.3 ± 0.2
$K_{-2f}^{(oG:C)}$ (s^{-1})	1.16 ± 0.02
$k_{3f}^{(oG:C)}$ (s^{-1})	0.012 ± 0.001
$K_{-3f}^{(oG:C)}$ (s^{-1})	0.07 ± 0.01
$k_{4f}^{(oG:C)}$ (s^{-1})	0.06 ± 0.02
$k_{5f}^{(oG:C)}$ (s^{-1})	0.0064 ± 0.0007

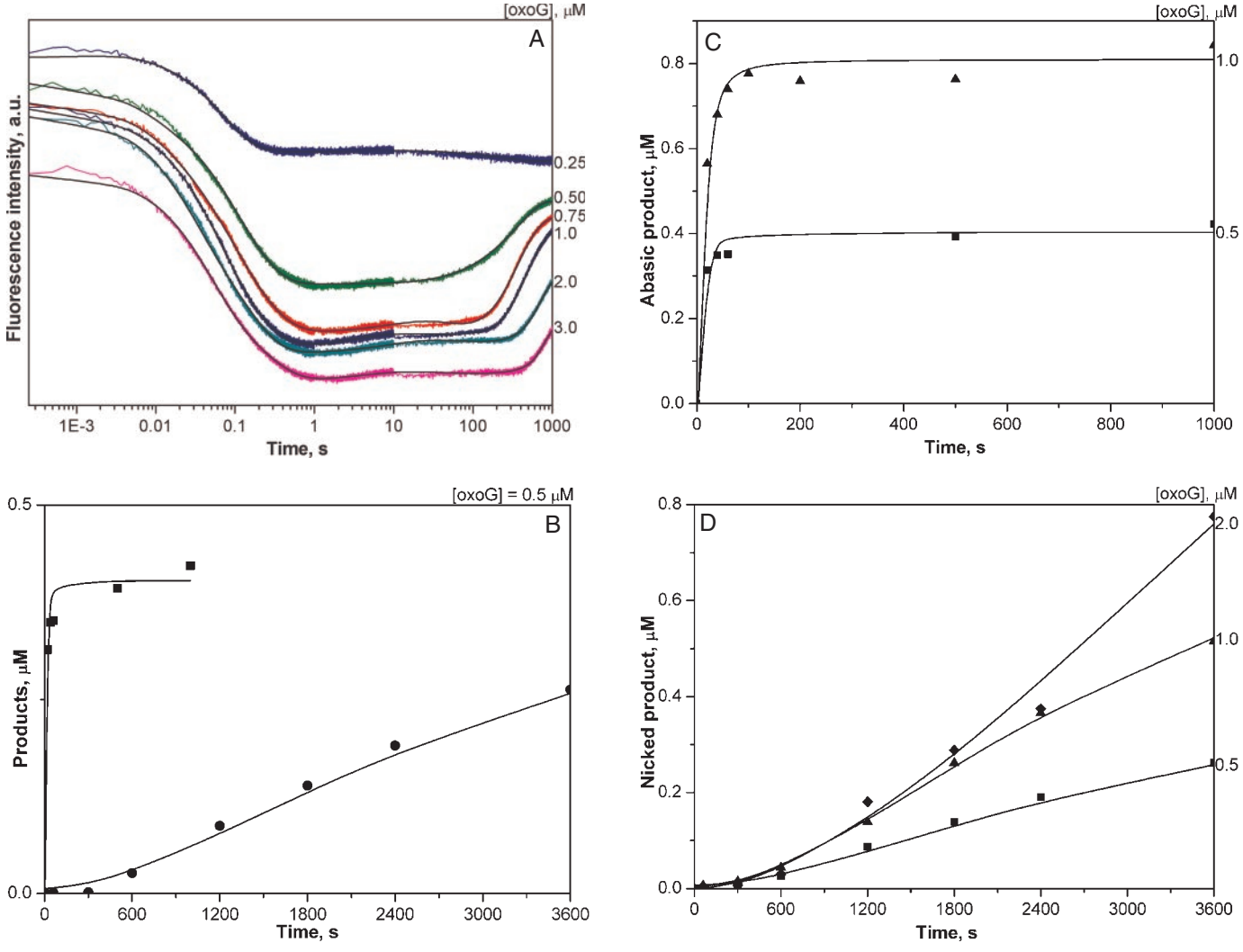

Figure 3. Binding and cleavage of the oxoG:C substrate by Ogg1. (**A**) Fluorescence traces for the overall reaction. Experimental data and fitting results are color-coded as in Figure 2. (**B**) Time course of accumulation of abasic (squares) and nicked (circles) products at 0.5 μM substrate concentration. (**C**) Time course of accumulation of the abasic product at 0.5 μM (squares) and 1 μM (triangles) substrate concentration. (**D**) Time course of the nicked product accumulation at 0.5 μM (squares), 1 μM (triangles) and 2 μM (diamonds) substrate concentration.

literature data on slow cleavage of the nascent AP site and slow product release by mammalian Ogg1 (24), the full reaction scheme (Scheme 1a) could possibly contain, after the initial three binding equilibria and two irreversible (chemical) steps, one equilibrium step corresponding to product release, characterized by the dissociation constant K_{EP}.

$$E + S \underset{k_{-1f}}{\overset{k_{1f}}{\rightleftharpoons}} ES1 \underset{k_{-2f}}{\overset{k_{2f}}{\rightleftharpoons}} ES2 \underset{k_{-3f}}{\overset{k_{3f}}{\rightleftharpoons}} ES3 \overset{k_{4f}}{\longrightarrow} EP1 \overset{k_{5f}}{\longrightarrow} EP2 \overset{K_{EP}}{\rightleftharpoons} E + P$$

Scheme 1a. Full reaction scheme for binding and cleavage of an 8-oxoG:C-containing substrate by Ogg1.

To determine the equilibrium constant KEP, if any, for product binding and release, we performed fluorescent titration of hOgg1. Since the true reaction product (containing a nick in DNA flanked by an α,β-unsaturated aldehyde at its 5′-side and a phosphate at the 3′-side) was hard to obtain in the required amounts, we instead used a dsODN containing a single-nucleotide gap flanked by two phosphates as a product analog:

CpTpCpTpCp pCpCpTpTpCpC

GpApGpApGpCpGpGpApApGpG

A single transition was observed at melting temperature, $T_m = 20.8°C$ in a melting curve of this ternary ODN system, indicating that less than a half of the complex would still be present under our experimental conditions (25°C). Thus, we titrated hOgg1 with an equimolar mixture of the three ODNs composing the gapped duplex and registered changes in the maximum of fluorescence spectrum of the protein. The resulting K_{EPt} value, 0.88×10^{-6} M (corrected for the total concentration of individual ODNs), approximates the true product equilibrium constant, which is also likely to be influenced by the presence of a 4-hydroxy-2-pentenal moiety in the true product.

In stopped-flow experiments with detection based on changes in intrinsic tryptophan fluorescence of protein molecules, only events associated with conformational changes in the Trp-containing enzyme parts could be detected. To assign discernible fluorescence changes to particular chemical steps of the Ogg1-catalyzed reaction, we used PAGE to follow the time course of accumulation of the abasic product (revealed by alkaline treatment of the reaction mixture) and of the nicked product during processing of 8-oxoG:C-containing duplex by Ogg1 (Figure 3B). The general association constant was calculated from fluorescence traces as $K_A = K_1 + K_1K_2 + K_1K_2K_3$ (where K_1, K_2 and K_3 are the equilibrium constants for the first three reversible steps in Scheme 1), and this value (2.9×10^7 M^{-1}) was used for fitting the data on the accumulation of abasic product to Scheme 2.

$$E + S \overset{K}{\rightleftharpoons} ES \overset{k_{2e}}{\longrightarrow} EP1$$

Scheme 2. Accumulation of abasic product.

From this scheme, k_{2e} was calculated as 0.08 s^{-1}. Then, using the calculated values and the data on the accumulation of the nicked product, the next kinetic constant k_{3e} could be estimated by fitting these parameters to Scheme 3.

$$E + S \overset{K}{\rightleftharpoons} ES \overset{k_{2e}}{\longrightarrow} EP1 \overset{k_{3e}}{\longrightarrow} EP2$$

Scheme 3. Accumulation of nicked product.

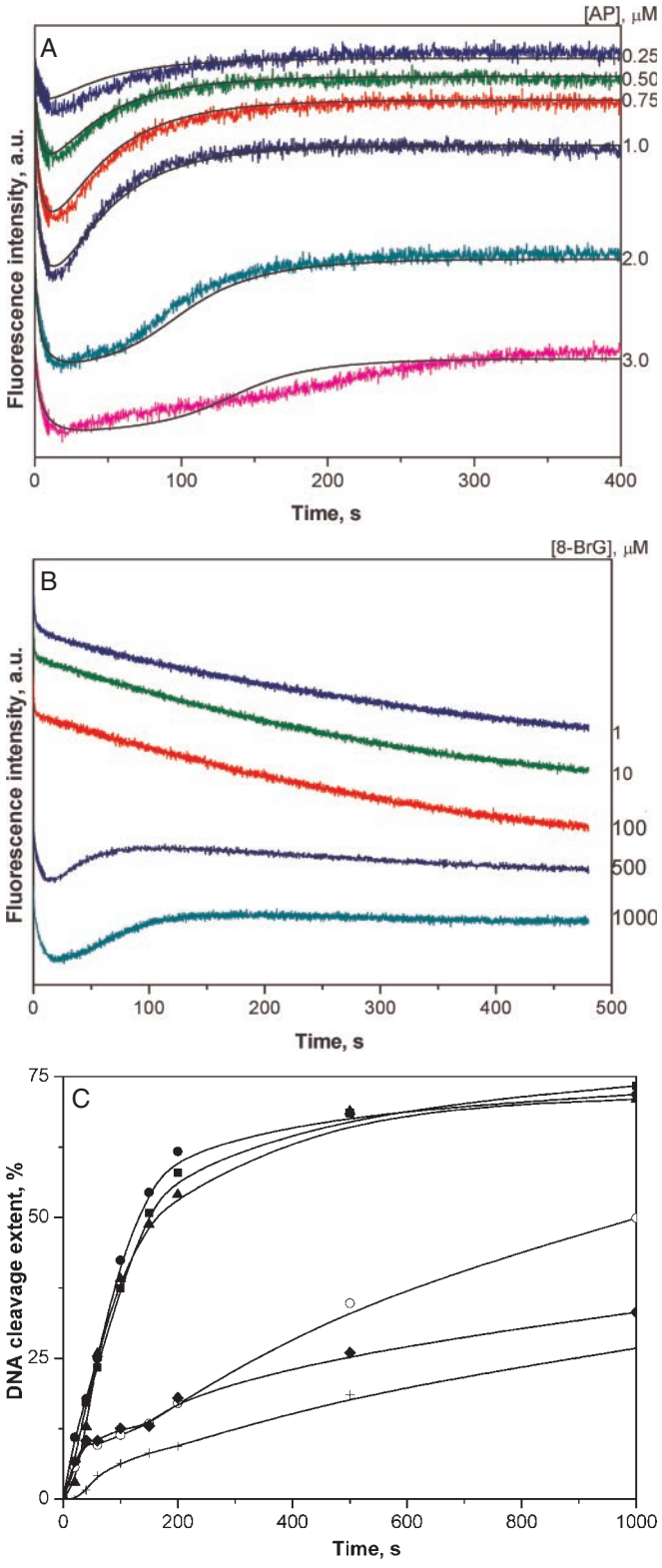

Figure 4. Binding and cleavage of the AP:C substrate by Ogg1 in the presence of 8-BrG. (**A**) fluorescence traces for the overall reaction at 0.5 mM 8-BrG, [hOgg1] = 1 μM. Experimental data and fitting results are color-coded as in Figure 2. (**B**) Dependence of the reaction on 8-BrG concentration; [AP:C] = 1 μM, [hOgg1] = 1 μM. (**C**) Time course of accumulation of nicked product at different substrate concentrations: [AP:C] = 0.5 μM (filled circles), 1 μM (squares), 2 μM (triangles), 15 μM (open circles), 20 μM (diamonds), 30 μM (crosses); [hOgg1] = 1 μM, [8-BrG] = 0.5 mM.

The calculated value for k_{3e} was (0.7–1.4) $\times 10^{-3}$ s^{-1}. Thus, it is clear that rate constant k_{2e} determined in the cleavage experiments corresponds to the k_{4f} constant determined in the fluorescence experiments (their values being 0.08 s^{-1} and 0.06 s^{-1}, respectively), and therefore the latter reflects the first chemical stage of the reaction, release of the damaged base. Accordingly, k_{3e} constant determined in the cleavage experiments most likely corresponds to the k_{5f} constant determined in the fluorescence experiments (0.001 s^{-1} and 0.006 s^{-1}, respectively; note that the error in k_{5f} was quite large due to a large contribution of fluorescence bleaching of the enzyme at the late stages of the reaction, which may explain the apparent 6-fold difference in the constants measured by the two methods), suggesting that k_{5f} is associated with the second chemical stage, β-elimination of the nascent AP site. The values of the irreversible rate constants and the difference between them agree well with the data reported for Michaelis–Menten approximation of the kinetics of mammalian Ogg1 (24,45). The correspondence of k_{4f} and k_{5f} to the irreversible chemical steps suggests that the preceding equilibrium stages reflect conformational equilibria during substrate recognition and Michaelis complex formation.

Effect of 8-BrG on the interaction of Ogg1 with AP:C- and 8-oxoG:C-containing duplexes

As discussed above, the interaction of Ogg1 with substrate containing an aldehydic AP site was essentially non-catalytic, with very little β-elimination at the AP site observed for up to 1000 s of the reaction course (Figure 2). Recent structural data suggested that proton abstraction at C2′, a step necessary for initiating β-elimination, is likely to be catalyzed by the anionic form of the damaged base immediately after dissociation of the glycosidic bond (30). Consistent with this, the overall reaction of AP site cleavage is accelerated by guanine analogues substituted at C8 with an electronegative moiety, such as 8-BrG (30). To analyze this process in detail, we obtained fluorescence traces of Ogg1 in the presence of AP:C substrate and 8-BrG (Figure 4A). Fluorescence titration data indicated that 8-BrG slightly facilitated non-specific binding of hOgg1 to DNA [$K_{ESt}^{(G:C,BrG)} = 0.67 \times 10^{-5}$ M; compare $K_{ESf}^{(G:C)} = 2.9 \times 10^{-5}$ M]. The addition of 8-BrG caused a drastic change in shapes of the fluorescent traces with the AP:C substrate, which now displayed a behavior characteristic of a regular reaction time course, with the fluorescence returning back to the starting values after some time. This change was dependent on the concentration of 8-BrG (Figure 4B). The reaction progressed as far as the reaction of Ogg1 with the 8-oxoG:C substrate being essentially complete after ~200 s. Binding of 8-BrG to Ogg1 in the absence of DNA was not accompanied by a significant fluorescence change even at saturating concentrations of the base (500 μM) (data not shown). Therefore, we used Scheme 4 to fit the data and obtain the values of the kinetic constants (listed in Table 2).

$$E + S \underset{k_{-1f}}{\overset{k_{1f}}{\rightleftharpoons}} ES1 \underset{k_{-2f}}{\overset{k_{2f}}{\rightleftharpoons}} ES2 \xrightarrow{k_{3f}} EP \overset{K_{EPf}}{\rightleftharpoons} E + P$$

Scheme 4. Binding and cleavage of an AP:C-containing substrate by Ogg1 in the presence of B-BrG.

The overall acceleration of the process caused the initial reaction steps to merge, resulting in only two discernible stages instead of three stages in Scheme 1. The time course of accumulation of the eliminated product (Figure 4C) shows that the characteristic time of strand cleavage correlates well with that obtained from the fluorescence data.

We also analyzed the effect of 8-BrG on the processing of the damaged base-containing 8-oxoG:C substrate by Ogg1. Addition of 8-BrG did not significantly modify fluorescence traces and the characteristic times of the equilibrium stages. However, two irreversible steps featured in Scheme 1 merged in a single fluorescently discernible stage with $k_{4f}^{(oG:C,BrG)} = 0.029$ s^{-1}, a 5-fold acceleration of the chemistry rate compared with the calculated overall chemistry rate (0.006 s^{-1}) (Table 3). Experiments with radioactively labeled substrate revealed a great increase in the rate of accumulation of the product with the DNA backbone cleaved (Figure 5).

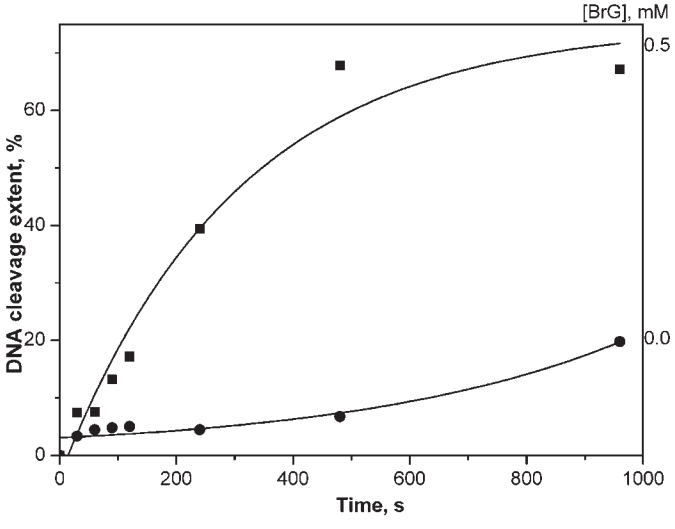

Figure 5. Enhancement of AP lyase activity of Ogg1 by 8-BrG on the 8-oxoG:C substrate. Time course of accumulation of nicked product is shown at concentration of 8-BrG 0.5 mM (squares) and without 8-BrG (circles).

Table 2. Rate constants for interactions of Ogg1 with AP:C in the presence of 8-BrG

Rate constant	Mean ± SD
$k_{1f}^{(AP:C,BrG)}$ (M^{-1} s^{-1})	(5.4 ± 0.7) × 10^8
$K_{-1f}^{(AP:C,BrG)}$ (s^{-1})	960 ± 40
$k_{2f}^{(AP:C,BrG)}$ (s^{-1})	1.5 ± 0.2
$K_{-2f}^{(AP:C,BrG)}$ (s^{-1})	0.059 ± 0.004
$k_{3f}^{(AP:C,BrG)}$ (s^{-1})	0.024 ± 0.001
$K_{EPf}^{(AP:C,BrG)}$ (M)	(2.8 ± 0.2) × 10^{-6}

Table 3. Rate constants for interactions of Ogg1 with 8-oxoG:C in the presence of 8-BrG

Rate constant	Mean ± SD
$k_{1f}^{(oG:C,BrG)}$ (M^{-1} s^{-1})	(2.12 ± 0.02) × 10^8
$K_{-1f}^{(oG:C,BrG)}$ (s^{-1})	167 ± 0.7
$k_{2f}^{(oG:C,BrG)}$ (s^{-1})	7.88 ± 0.03
$K_{-2f}^{(oG:C,BrG)}$ (s^{-1})	1.19 ± 0.01
$k_{3f}^{(oG:C,BrG)}$ (s^{-1})	0.03 ± 0.001
$K_{-3f}^{(oG:C,BrG)}$ (s^{-1})	0.27 ± 0.02
$k_{4f}^{(oG:C,BrG)}$ (s^{-1})	0.029 ± 0.001
$K_{EPf}^{(oG:C,BrG)}$ (M)	(2.1 ± 0.3) × 10^{-5}

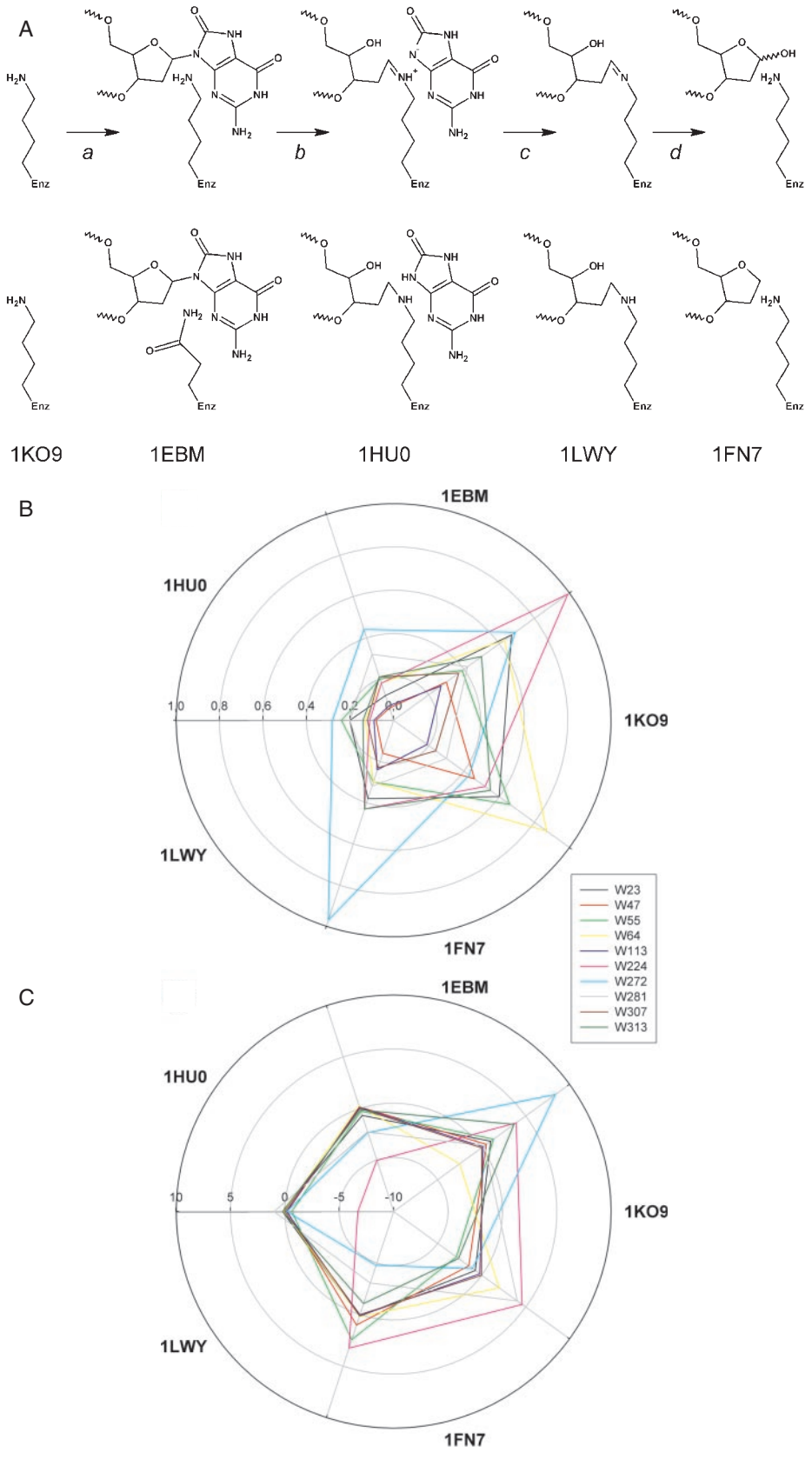

Figure 6. (**A**) Events occurring in the Ogg1 active site during the catalytic cycle (top row) and the structures mimicking the respective reaction steps (bottom row): *a*, binding of 8-oxodG; *b*, 8-oxoG excision with the formation of a Schiff base; *c*, departure of the excised 8-oxoG; *d*, hydrolysis of the Schiff base. (**B**) Changes in the position of individual Trp residues during catalysis, calculated from the respective structures. R.m.s.d. (Å along the radial axis) between any two adjacent structures is shown. (**C**) Changes (Å^2 along the radial axis) in the solvent-accessible area of individual Trp residues during catalysis, calculated from the respective structures.

DISCUSSION

Structural basis for Ogg1 fluorescence

The 3D structure of Ogg1 has been determined for the free enzyme (46), the complex of a catalytically inactive K249Q Ogg1 with an 8-oxoG-containing oligonucleotide duplex (42), the complex of wild-type Ogg1 with an uncleavable F-containing duplex (43) and the $NaBH_4$-reduced covalent complex (30). The Ogg1 molecule contains 10 tryptophan residues, many of which are partially exposed to the surface and located in those regions of the protein globule that can be reasonably expected to be rather flexible. Structural features of the Ogg1 molecule moving along the reaction coordinate can be revealed by comparing these structures.

To reveal movements of tryptophan residues and changes in their environment, we analyzed the following Ogg1 structures: 1KO9 [free enzyme (46)], 1EBM [K249Q Ogg1 complexed with an 8-oxoG-containing duplex (42)], 1HU0 [Ogg1 cross-linked to C1′ of deoxyribitol, with 8-oxoG base still present in the active site (30)], 1LWY [Ogg1 cross-linked to C1′ of deoxyribitol, with 8-oxoG base dissociated from the active site (30)] and 1FN7 [Ogg1 complexed with an tetrahydrofuran analogue of an abasic site (43)]. Thus, sampling of the series 1KO9→ 1EBM→1HU0→1LWY→1FN7→1KO9 provides a model of five of the stages of the full Ogg1 catalytic cycle (disregarding the inefficient β-elimination step; Figure 6A), whereas 1KO9→ 1FN7→1KO9 is a model for binding F:C and AP:C.

We have analyzed the movement of all tryptophan residues (in terms of r.m.s.d. between two structures adjacent in the reaction path), as well as the changes in their water-accessible surfaces. Figure 6B and C shows that Trp224 and Trp272 are likely to be the most informative Trp residues in fluorescence kinetic studies, demonstrating the largest amplitude of changes during the full catalytic cycle. On the other hand, the binding of Ogg1 to an F:C duplex is expected to be accompanied by a more pronounced signal from Trp55 and Trp272 and probably Trp64 and Trp313, but not Trp224. Trp224 and Trp272 occur in the surface helices of Ogg1 (αJ and αM, respectively) that can be quite sensitive to DNA binding in general and to conformational changes in the DNA. In fact, one of these residues, Trp272, has been proposed to participate in a hinge movement of a Pro266–Trp272 loop that activates a critical catalytic residue Asp268 (46). Trp224 participates in the packing of an extensive helical region encompassing a helix(αK)–hairpin–helix(αL) motif that harbors the catalytic Lys249 residue (42,43). Trp55, Trp64 and Trp313 are more distal to DNA, lying at the opposite surface of the protein globule, and a change in their fluorescence is likely to reflect just DNA binding in general. Thus, it is likely that in the absence of cofactors, such as 8-BrG, we observe only DNA binding and release in the case of F:C, AP:C, and probably G:C. More subtle DNA dynamics and catalytically important rearrangements in the protein molecule, namely in the αJ–αM helices, are revealed for 8-oxoG:C and AP:C in the presence of 8-BrG, manifesting themselves as individually detectable fluorescence change steps.

Kinetic model attribution

The general scheme for lesion recognition and excision by DNA glycosylases (47) includes seven principal steps: (i) binding to an undamaged DNA stretch; (ii) sliding along DNA in a search for a lesion; (iii) recognition of a lesion in double-stranded DNA; (iv) eversion of the damaged nucleotide into the active site pocket and insertion of specific enzyme residues in the resulting void in DNA; (v) adjustment of the enzyme and DNA conformation to that optimal for catalysis; (vi) one or more catalytic steps leading to base excision and possibly DNA strand cleavage; and (vii) product release. Characteristic times of these processes may be vastly different. For instance, binding of DNA glycosylases to DNA and sliding along DNA are very rapid (36,37,47–51), whereas product release in extreme cases may take hours (52).

We have found that the kinetic scheme for Ogg1 acting on a 8-oxoG:C-containing substrate includes at least three fast equilibrium steps followed by two slow irreversible steps, followed in turn by one more equilibrium step. The second irreversible step was rate-limiting for the complete reaction. By comparing the data derived from Ogg1 intrinsic fluorescence traces and from accumulation of products of different types, we attributed the irreversible steps to two main chemical steps of the Ogg1-catalyzed reaction, namely the cleavage of the *N*-glycosidic bond of the damaged nucleotide and β-elimination of its 3′-phosphate. Both the absolute values and the ratio of the respective constants are in good agreement with the values determined by steady-state kinetics for murine Ogg1 (24).

The nature of first three equilibria is harder to define unequivocally, but reasonable suggestions can be made in this case. First, the lack of discernible fluorescence change events during Ogg1 binding to non-specific DNA suggests that recognition steps A and B (see above) are likely not to be detected in our experiments with cleavable substrates. The characteristic time of binding to non-specific DNA was considerably longer than to 8-oxoG-containing DNA. In fact, non-specific binding and sliding was not detected as discernible events in pre-steady-state kinetic studies of other DNA glycosylases, including uracil–DNA glycosylase, Fpg, and MutY (36,37,47–51), most probably because of very small size of oligonucleotide targets used in this technique. The first equilibrium step thus reflects the equilibrium between free enzyme plus DNA and the complex that is already specific, with the process of lesion recognition commenced. Base eversion, void-filling and enzyme conformation adjustment likely underlie the second and third equilibrium steps.

The last equilibrium step must correspond to product release, raising an interesting question about the nature of the released product. In principle, Ogg1 may be in equilibrium with both the abasic product with the intact backbone and the product in which the backbone has been nicked. However, we found that introduction of an equilibrium step for release and binding of AP-DNA worsened the data fit. In addition, Monte Carlo simulation of the complete Ogg1 reaction time course suggests that the rate constant of Ogg1 dissociation from its abasic product must be extremely low (D. O. Zharkov, manuscript in preparation). This dramatic difference between dissociation of AP-DNA formed *de novo* by 8-oxoG excision and AP-DNA bound from solution may be explained by the persistence of the Schiff base after 8-oxoG excision, efficiently anchoring Ogg1 to its product, or by conformational differences in the Ogg1/AP-DNA complex originated by these different routes. Since we did not observe AP:C cleavage

unassisted by 8-BrG, the K_{EPf} value for the last step of the reaction with AP:C in the presence of 8-BrG (2.8×10^{-6} M) may provide a good estimate for the affinity for the nicked unsaturated aldehyde product. This value is higher than K_{EPt} determined by titration with a gapped product (0.88×10^{-6} M) and higher than K_{ESf} for the AP:C substrate (0.24×10^{-6} M), making it likely that the nicked product dissociates faster in the presence of the excised base.

When AP:C substrate and 8-BrG were used as a model system, the reaction was most adequately described by two initial equilibrium steps and one irreversible chemical step plus the final product release equilibrium step. The nature of the reversible steps is likely similar to those in the case of 8-oxoG:C, with the caveat that the structural differences mentioned in a previous section allow observation of fewer conformational changes. The irreversible step may correspond to Schiff base formation or β-elimination; the latter possibility is more likely since β-elimination is the step accelerated by 8-BrG.

Stimulation of Ogg1 by 8-BrG

Structural and kinetic evidence (30) point at the just-excised base in its anionic form as the basic acceptor for a proton at C2′ of the damaged nucleotide to initiate β-elimination following the base excision step. 8-Substituted derivatives of guanine (8-BrG, 8-aminoguanine) and even guanine itself have been demonstrated to accelerate nicking at the AP sites by Ogg1. We have confirmed these observations in stopped-flow experiments, showing that the rate of β-elimination step with the AP:C substrate increases at least several orders of magnitude in the presence of 8-BrG, from virtually undetectable to 0.024 s^{-1}.

A much less expected finding was that 8-BrG also significantly enhanced the AP lyase activity on the 8-oxoG-containing substrate. In the case of this substrate, the excised 8-oxoG base is expected to be retained in the enzyme's active site pocket for a considerable time, enough to allow crystallization of the enzyme with the excised base still associated with it (30). Given the tightness of the base-accommodating pocket of Ogg1 (42), it is very unlikely that 8-BrG can be bound in the pocket first and still retained there after the 8-oxoG moiety is everted from DNA in the process of catalysis. If anything, binding of 8-BrG in the pocket before binding the oligonucleotide would show up as competitive inhibition of the overall reaction. We believe that the observed increase in AP lyase activity could be explained most reasonably by a rapid equilibrium step after base excision, allowing for a quick exchange between the excised 8-oxoG in the active site pocket and 8-BrG outside of the enzyme–DNA complex. The lack of change in tryptophan fluorescence on 8-BrG binding to the enzyme globule suggests that this equilibrium could be invisible in our fluorescence traces. Base excision could lead to a local destabilization of one of the walls of the active site pocket allowing the excised lesion to diffuse away, as proposed for the bacterial 8-oxoG glycosylase Fpg (20). This enzyme conformational change may persist after the purine base exchange, leading to destabilization of the complex and providing a possible explanation for a lower affinity for the product formed from the 8-oxoG-containing substrate compared with the product formed from the AP-containing substrate (compare K_{EPf} values of 2.8×10^{-6} M for AP:C in the presence of 8-BrG and 2.1×10^{-5} M for 8-oxoG:C in the presence of 8-BrG). When no free base is present in solution, a very low solubility of 8-oxoG base could still lead to the equilibrium favoring the presence of 8-oxoG in the pocket (and thus making it visible in the crystal structure), whereas simple mass action would shift the balance in favor of 8-BrG in the pocket if 8-BrG is present in saturating concentrations in the solution. 8-BrG could also act as an allosteric activator of the AP lyase activity, but we hold this possibility less likely, since no structural basis for such interactions is revealed by the Ogg1 structures (30,42,43,46).

Although our experiments support the mechanism of product-assisted catalysis of β-elimination, as proposed by Verdine and co-workers (30), under normal conditions (i.e. in the absence of externally added guanine derivatives) nicking of DNA by Ogg1 is still very inefficient even when the substrate contains the damaged base, a precursor of the catalytic moiety (Figure 3B). Therefore, 8-oxoG anion is either rapidly protonated at N9 or diffuses from the active site pocket, as discussed above, no longer capable of fulfilling its proton acceptor role. The activity of Ogg1 was shown to be stimulated by AP endonucleases (44,53,54); this process likely involves active displacement of Ogg1 from the complex with its AP site product and cleavage of the AP site by AP endonuclease (D. O. Zharkov, manuscript in preparation). Thus, we argue that the product-assisted catalysis by Ogg1, despite being interesting mechanistically, is probably irrelevant to the situation *in vivo*.

Comparison with bacterial 8-oxoG-DNA glycosylase Fpg

Fpg and Ogg1 are major 8-oxoG-DNA glycosylases in organisms belonging to the kingdoms Bacteria and Eukaryota, respectively. For both enzymes, 8-oxoG and FapyGua are the physiological substrates (25,27), although excision of many other bases from short oligonucleotides have been reported (20,31). Nevertheless, Fpg and Ogg1 are completely different in their sequence (15,19), structure (42,55) and do not fully overlap in their substrate specificity (23–27). Thus, comparing the kinetic schemes of these two enzymes on the same set of substrates is of great interest for understanding the mechanisms of recognition and repair of oxidative purine lesions. Toward this goal, we have used the same substrate system as we did previously for *E.coli* Fpg (36,37).

The most drastic differences between Fpg and Ogg1 were found, as expected from the earlier steady-state kinetic studies (23,24), during the chemical steps of the enzymatic reaction. For Fpg, which proceeds through three concerted chemical steps (base excision, β-elimination and δ-elimination), they were fast and could not be separated, observed as a single irreversible reaction in the complete reaction scheme (37). In contrast, the complete reaction scheme of Ogg1 clearly included two irreversible reactions, attributed to the base excision and β-elimination steps and characterized by the rate constants that differed about an order of magnitude. The β-elimination step was accelerated in the presence of 8-BrG, whereas this base had no effect on Fpg (37). Structurally this difference between the two enzymes in the efficiency of the β-elimination step can be interpreted from the

differences in coordination and neutralization of the leaving 3′-phosphate (20).

Recognition of 8-oxoG by Ogg1 and Fpg also proved to be different. When Fpg was acting on a 8-oxoG:C substrate, at least five equilibria were observed before chemical steps ensued, whereas with Ogg1 we found only three reversible steps. The first of these steps, reflecting binding of the enzyme to the substrate, was characterized by similar kinetic constants for both Ogg1 and Fpg, and for both 8-oxoG:C and AP:C substrates (compare the values for forward rates $k_1 = 3.2 \times 10^8$ M^{-1} s^{-1} for Fpg/8-oxoG:C, 8.0×10^8 M^{-1} s^{-1} for Fpg/AP:C, 2.6×10^8 M^{-1} s^{-1} for Ogg1/8-oxoG:C and 5.4×10^8 M^{-1} s^{-1} for Ogg1/AP:C, and the reverse rates k_{-1} = 890 s^{-1} for Fpg/8-oxoG:C, 250 s^{-1} for Fpg/AP:C, 130 s^{-1} for Ogg1/8-oxoG:C and 960 s^{-1} for Ogg1/AP:C; the values for Ogg1/AP:C are given for the 8-BrG-containing reaction). Thus, the primary encounter, translocation to the lesion and the first stage of lesion recognition are performed by Fpg and Ogg1 in similar ways, raising the possibility that lesion recognition is initially governed by the nature of the common substrate, 8-oxoG. For Fpg, it has recently been suggested from structural and site-directed mutagenesis data (31) that the initial stage of lesion recognition involves application of DNA-distorting force by the enzyme, and that only 'weak points' in DNA are probed further in the enzyme's active site; this scheme could probably be applied to Ogg1 as well. Since the forward rates are approaching the diffusion limit ($\sim 10^9$ M^{-1} s^{-1}), we suggest that formation of the primary encounter complex does not involve gross conformational changes in either Fpg or Ogg1, and that the 1D translocation is of limited significance with the short substrates used in this study.

The remaining two equilibria in Ogg1 and four equilibria in Fpg reflect conformational changes associated with flipping the target nucleotide out of DNA helix and adjustment of protein and DNA to the conformation optimal for catalysis. Obviously, differences in 3D structures of Ogg1 and Fpg preclude direct comparison of these processes. Nevertheless, several interesting features are evident from the observed kinetics. For example, the equilibrium in the last pre-chemical step in Ogg1-catalyzed reaction is shifted toward ES2 rather than ES3 (Scheme 1), making the immediate pre-catalytic complex a rather minor species in the complete reaction scheme at all times. In Fpg (37), with its five equilibrium steps, the third equilibrium is shifted to the left in similar manner, and the respective complex, ES2, also predominates for most of the reaction; however, in Fpg the immediate pre-catalytic complex eventually takes over. Thus, in both Fpg and Ogg1 the rate-limiting step in lesion recognition (as opposed to the overall reaction, including catalytic steps) is the conversion of ES2 to ES3, and ES2 is the complex contributing most to the process of recognition. There are reasons to believe that ES1 detected in pre-steady-state kinetic experiments with DNA glycosylases represents the conformation immediately preceding damaged nucleotide eversion (49,51); the next step would therefore correspond to the eversion, which could precede insertion of the void-filling residues stabilizing the everted conformation (51). Thus, we suggest that the critical conformation in lesion discrimination is the complex of the enzyme with the everted but not yet fully stabilized 8-oxoG nucleotide (corresponding to ES2 in the kinetic scheme), in both Fpg and Ogg1.

After the eversion, several additional equilibrium steps are observed in Fpg, compared with only one for Ogg1. Although this may be related to the failure to observe certain conformational changes not associated with changes in tryptophan fluorescence, another possible explanation is more interesting. The base-binding pocket in Ogg1 is well-formed and tight (42), and thus little protein movement may be required to accommodate the everted damaged base. On the other hand, the pocket in Fpg is flexible and highly dynamic (20,31,56), allowing Fpg to excise a great repertoire of damaged bases (20), and several profound movements may be required to accommodate a given base in a conformation poised for catalysis. Despite all differences in the number of pre-chemical equilibrium steps, the characteristic time of accumulation of the final pre-chemical complex is similar for both Ogg1 and Fpg; this complex reaches half of its maximum concentration in $\sim$5 s after the reaction start.

Similar to other DNA glycosylases and DNA polymerases, hOgg1 seems to undergo a multistep open-to-closed conformational transition during substrate binding and further conformational changes during catalysis. Such behavior illustrates the concept of the dynamic model of enzyme catalysis (57), in which conformational changes in the enzyme molecule drive the substrate-to-product conversion. Ongoing experiments addressing hOgg1 reaction dynamics with substrates containing other modified purines and complementary bases should improve our understanding of the mechanism of lesion recognition by this repair enzyme.

SUPPLEMENTARY MATERIAL

Supplementary Material is available at NAR Online.

ACKNOWLEDGEMENTS

The authors are grateful to Dr Dmitri Pyshnyi for his invaluable help in the synthesis of substrates. The authors thank Ms Elena I. Zaika and Ms Tatiana A. Dudareva for their assistance in cloning and purification of hOgg1. This research was made possible in part by grants from the Wellcome Trust (UK) (070244/Z/03/Z), Presidium of the Russian Academy of Sciences (MCB Program, 10.5), RFBR (04-04-48171, 05-04-48619), the Russian Ministry of Education and Science (8256), NS-1419.2003.4, CRDF (REC-008, Y1-B-08-16). D.O.Z. is a recipient of the Best Young Investigator Fellowship from the Russian Science Support Foundation. V.V.K. was supported by Post Doctoral Fellowship from INTAS (04-83-3849). Funding to pay the Open Access publication charges for this article was provided by the Wellcome Trust (UK).

Conflict of interest statement. None declared.

REFERENCES

1. Halliwell,B. and Gutteridge,J.M.C. (1989) *Free Radicals in Biology and Medicine*, *2nd edn.* Clarendon Press, Oxford.
2. von Sonntag,C. (1987) *The Chemical Basis of Radiation Biology*. Taylor & Francis, London, New York, Philadelphia.

3. Burrows,C.J. and Muller,J.G. (1998) Oxidative nucleobase modifications leading to strand scission. *Chem. Rev*., **98**, 1109–1152.
4. Pogozelski,W.K. and Tullius,T.D. (1998) Oxidative strand scission of nucleic acids: routes initiated by hydrogen abstraction from the sugar moiety. *Chem. Rev*., **98**, 1089–1108.
5. Gajewski,E., Rao,G., Nackerdien,Z. and Dizdaroglu,M. (1990) Modification of DNA bases in mammalian chromatin by radiation-generated free radicals. *Biochemistry*, **29**, 7876–7882.
6. Shibutani,S., Takeshita,M. and Grollman,A.P. (1991) Insertion of specific bases during DNA synthesis past the oxidation-damaged base 8-oxodG. *Nature*, **349**, 431–434.
7. Shibutani,S., Bodepudi,V., Johnson,F. and Grollman,A.P. (1993) Translesional synthesis on DNA templates containing 8-oxo-7, 8-dihydrodeoxyadenosine. *Biochemistry*, **32**, 4615–4621.
8. Wiederholt,C.J. and Greenberg,M.M. (2002) Fapy dG instructs Klenow exo(−) to misincorporate deoxyadenosine. *J. Am. Chem. Soc*., **124**, 7278–7279.
9. Delaney,M.O., Wiederholt,C.J. and Greenberg,M.M. (2002) Fapy•dA induces nucleotide misincorporation translesionally by a DNA polymerase. *Angew. Chem. Int. Ed. Engl*., **41**, 771–773.
10. Michaels,M.L. and Miller,J.H. (1992) The GO system protects organisms from the mutagenic effect of the spontaneous lesion 8-hydroxyguanine (7,8-dihydro-8-oxoguanine). *J. Bacteriol*., **174**, 6321–6325.
11. Grollman,A.P. and Moriya,M. (1993) Mutagenesis by 8-oxoguanine: an enemy within. *Trends Genet*., **9**, 246–249.
12. Tajiri,T., Maki,H. and Sekiguchi,M. (1995) Functional cooperation of MutT, MutM and MutY proteins in preventing mutations caused by spontaneous oxidation of guanine nucleotide in *Escherichia coli*. *Mutat. Res*., **336**, 257–267.
13. Sakumi,K., Furuichi,M., Tsuzuki,T., Kakuma,T., Kawabata,S., Maki,H. and Sekiguchi,M. (1993) Cloning and expression of cDNA for a human enzyme that hydrolyzes 8-oxo-dGTP, a mutagenic substrate for DNA synthesis. *J. Biol. Chem*., **268**, 23524–23530.
14. Slupska,M.M., Baikalov,C., Luther,W.M., Chiang,J.-H., Wei,Y.-F. and Miller,J.H. (1996) Cloning and sequencing a human homolog (hMYH) of the *Escherichia coli* mutY gene whose function is required for the repair of oxidative DNA damage. *J. Bacteriol*., **178**, 3885–3892.
15. Auffret van der Kemp,P., Thomas,D., Barbey,R., de Oliveira,R. and Boiteux,S. (1996) Cloning and expression in *Escherichia coli* of the *OGG1* gene of *Saccharomyces cerevisiae*, which codes for a DNA glycosylase that excises 7,8-dihydro-8-oxoguanine and 2,6-diamino-4-hydroxy-5-N-methylformamidopyrimidine. *Proc. Natl Acad. Sci. USA*, **93**, 5197–5202.
16. Rosenquist,T.A., Zharkov,D.O. and Grollman,A.P. (1997) Cloning and characterization of a mammalian 8-oxoguanine DNA glycosylase. *Proc. Natl Acad. Sci. USA*, **94**, 7429–7434.
17. Thayer,M.M., Ahern,H., Xing,D., Cunningham,R.P. and Tainer,J.A. (1995) Novel DNA binding motifs in the DNA repair enzyme endonuclease III crystal structure. *EMBO J*., **14**, 4108–4120.
18. Nash,H.M., Bruner,S.D., Schärer,O.D., Kawate,T., Addona,T.A., Spooner,E., Lane,W.S. and Verdine,G.L. (1996) Cloning of a yeast 8-oxoguanine DNA glycosylase reveals the existence of a base-excision DNA-repair protein superfamily. *Curr. Biol*., **6**, 968–980.
19. Michaels,M.L., Pham,L., Cruz,C. and Miller,J.H. (1991) MutM, a protein that prevents G.C→T.A transversions, is formamidopyrimidine-DNA glycosylase. *Nucleic Acids Res*., **19**, 3629–3632.
20. Zharkov,D.O., Shoham,G. and Grollman,A.P. (2003) Structural characterization of the Fpg family of DNA glycosylases. *DNA Repair (Amst.)*, **2**, 839–862.
21. Zharkov,D.O., Rieger,R.A., Iden,C.R. and Grollman,A.P. (1997) NH_2-terminal proline acts as a nucleophile in the glycosylase/AP-lyase reaction catalyzed by *Escherichia coli* formamidopyrimidine-DNA glycosylase (Fpg) protein. *J. Biol. Chem*., **272**, 5335–5341.
22. Nash,H.M., Lu,R., Lane,W.S. and Verdine,G.L. (1997) The critical active-site amine of the human 8-oxoguanine DNA glycosylase, hOgg1: direct identification, ablation and chemical reconstitution. *Chem. Biol*., **4**, 693–702.
23. Tchou,J., Bodepudi,V., Shibutani,S., Antoshechkin,I., Miller,J., Grollman,A.P. and Johnson,F. (1994) Substrate specificity of Fpg protein. Recognition and cleavage of oxidatively damaged DNA. *J. Biol. Chem*., **269**, 15318–15324.
24. Zharkov,D.O., Rosenquist,T.A., Gerchman,S.E. and Grollman,A.P. (2000) Substrate specificity and reaction mechanism of murine 8-oxoguanine-DNA glycosylase. *J. Biol. Chem*., **275**, 28607–28617.
25. Karakaya,A., Jaruga,P., Bohr,V.A., Grollman,A.P. and Dizdaroglu,M. (1997) Kinetics of excision of purine lesions from DNA by *Escherichia coli* Fpg protein. *Nucleic Acids Res*., **25**, 474–479.
26. Boiteux,S., Gajewski,E., Laval,J. and Dizdaroglu,M. (1992) Substrate specificity of the *Escherichia coli* Fpg protein (formamidopyrimidine-DNA glycosylase): excision of purine lesions in DNA produced by ionizing radiation or photosensitization. *Biochemistry*, **31**, 106–110.
27. Dherin,C., Radicella,J.P., Dizdaroglu,M. and Boiteux,S. (1999) Excision of oxidatively damaged DNA bases by the human alpha-hOgg1 protein and the polymorphic alpha-hOgg1(Ser326Cys) protein which is frequently found in human populations. *Nucleic Acids Res*., **27**, 4001–4007.
28. Dizdaroglu,M. (2003) Substrate specificities and excision kinetics of DNA glycosylases involved in base-excision repair of oxidative DNA damage. *Mutat. Res*., **531**, 109–126.
29. Bjørås,M., Luna,L., Johnsen,B., Hoff,E., Haug,T., Rognes,T. and Seeberg,E. (1997) Opposite base-dependent reactions of a human base excision repair enzyme on DNA containing 7,8-dihydro-8-oxoguanine and abasic sites. *EMBO J*., **16**, 6314–6322.
30. Fromme,J.C., Bruner,S.D., Yang,W., Karplus,M. and Verdine,G.L. (2003) Product-assisted catalysis in base-excision DNA repair. *Nature Struct. Biol*., **10**, 204–211.
31. Zaika,E.I., Perlow,R.A., Matz,E., Broyde,S., Gilboa,R., Grollman,A.P. and Zharkov,D.O. (2004) Substrate discrimination by formamidopyrimidine-DNA glycosylase: a mutational analysis. *J. Biol. Chem*., **279**, 4849–4861.
32. Lesser,D.R., Kurpiewski,M.R. and Jen-Jacobson,L. (1990) The energetic basis of specificity in the EcoRI endonuclease-DNA interaction. *Science*, **250**, 776–786.
33. Nevinsky,G.A. (2003) Structural, thermodynamic, and kinetic basis of DNA- and RNA-dependent enzymes functioning. Important role of weak nonspecific additive interactions between enzymes and long nucleic acids for their recognition and transformation. In Uversky,V.N. (ed.), *Protein Structures: Kaleidoscope of Structural Properties and Functions*. Research Signpost, Kerala, Vol. 37/661, pp. 133–222.
34. Beloglazova,N.G., Kirpota,O.O., Starostin,K.V., Ishchenko,A.A., Yamkovoy,V.I., Zharkov,D.O., Douglas,K.T. and Nevinsky,G.A. (2004) Thermodynamic, kinetic and structural basis for recognition and repair of abasic sites in DNA by apurinic/apyrimidinic endonuclease from human placenta. *Nucleic Acids Res*., **32**, 5134–5146.
35. Zharkov,D.O., Ishchenko,A.A., Douglas,K.T. and Nevinsky,G.A. (2003) Recognition of damaged DNA by *Escherichia coli* Fpg protein: insights from structural and kinetic data. *Mutat. Res*., **531**, 141–156.
36. Fedorova,O.S., Nevinsky,G.A., Koval,V.V., Ishchenko,A.A., Vasilenko,N.L. and Douglas,K.T. (2002) Stopped-flow kinetic studies of the interaction between *Escherichia coli* Fpg protein and DNA substrates. *Biochemistry*, **41**, 1520–1528.
37. Koval,V.V., Kuznetsov,N.A., Zharkov,D.O., Ishchenko,A.A., Douglas,K.T., Nevinsky,G.A. and Fedorova,O.S. (2004) Pre-steady-state kinetics shows differences in processing of various DNA lesions by *Escherichia coli* formamidopyrimidine-DNA glycosylase. *Nucleic Acids Res*., **32**, 926–935.
38. Long,R.A., Robins,R.K. and Townsend,L.B. (1967) Purine nucleosides. XV. The synthesis of 8-amino- and 8-substituted aminopurine nucleosides. *J. Org. Chem*., **32**, 2751–2756.
39. Kuzmic,P. (1996) Program DYNAFIT for the analysis of enzyme kinetic data: application to HIV proteinase. *Anal. Biochem*., **237**, 260–273.
40. Guex,N. and Peitsch,M.C. (1997) SWISS-MODEL and the Swiss-PdbViewer: an environment for comparative protein modeling. *Electrophoresis*, **18**, 2714–2723.
41. Fraczkiewicz,R. and Braun,W. (1998) Exact and efficient analytical calculation of the accessible surface areas and their gradients for macromolecules. *J. Comput. Chem*., **19**, 319–333.
42. Bruner,S.D., Norman,D.P. and Verdine,G.L. (2000) Structural basis for recognition and repair of the endogenous mutagen 8-oxoguanine in DNA. *Nature*, **403**, 859–866.
43. Norman,D.P.G., Bruner,S.D. and Verdine,G.L. (2001) Coupling of substrate recognition and catalysis by a human base-excision DNA repair protein. *J. Am. Chem. Soc*., **123**, 359–360.
44. Hill,J.W., Hazra,T.K., Izumi,T. and Mitra,S. (2001) Stimulation of human 8-oxoguanine-DNA glycosylase by AP-endonuclease: potential coordination of the initial steps in base excision repair. *Nucleic Acids Res*., **29**, 430–438.

45. Audebert,M., Radicella,J.P. and Dizdaroglu,M. (2000) Effect of single mutations in the *OGG1* gene found in human tumors on the substrate specificity of the Ogg1 protein. *Nucleic Acids Res.*, **28**, 2672–2678.
46. Bjørås,M., Seeberg,E., Luna,L., Pearl,L.H. and Barrett,T.E. (2002) Reciprocal 'flipping' underlies substrate recognition and catalytic activation by the human 8-oxo-guanine DNA glycosylase. *J. Mol. Biol.*, **317**, 171–177.
47. Stivers,J.T. and Jiang,Y.L. (2003) A mechanistic perspective on the chemistry of DNA repair glycosylases. *Chem. Rev.*, **103**, 2729–2759.
48. Stivers,J.T., Pankiewicz,K.W. and Watanabe,K.A. (1999) Kinetic mechanism of damage site recognition and uracil flipping by *Escherichia coli* uracil DNA glycosylase. *Biochemistry*, **38**, 952–963.
49. Jiang,Y.L. and Stivers,J.T. (2002) Mutational analysis of the base-flipping mechanism of uracil DNA glycosylase. *Biochemistry*, **41**, 11236–11247.
50. Bernards,A.S., Miller,J.K., Bao,K.K. and Wong,I. (2002) Flipping duplex DNA inside out: a double base-flipping reaction mechanism by *Escherichia coli* MutY adenine glycosylase. *J. Biol. Chem.*, **277**, 20960–20964.
51. Wong,I., Lundquist,A.J., Bernards,A.S. and Mosbaugh,D.W. (2002) Presteady-state analysis of a single catalytic turnover by *Escherichia coli* uracil-DNA glycosylase reveals a 'pinch-pull-push' mechanism. *J. Biol. Chem.*, **277**, 19424–19432.
52. Zharkov,D.O. and Grollman,A.P. (1998) MutY DNA glycosylase: base release and intermediate complex formation. *Biochemistry*, **37**, 12384–12394.
53. Vidal,A.E., Hickson,I.D., Boiteux,S. and Radicella,J.P. (2001) Mechanism of stimulation of the DNA glycosylase activity of hOGG1 by the major human AP endonuclease: bypass of the AP lyase activity step. *Nucleic Acids Res.*, **29**, 1285–1292.
54. Saitoh,T., Shinmura,K., Yamaguchi,S., Tani,M., Seki,S., Murakami,H., Nojima,Y. and Yokota,J. (2001) Enhancement of OGG1 protein AP lyase activity by increase of APEX protein. *Mutat. Res.*, **486**, 31–40.
55. Sugahara,M., Mikawa,T., Kumasaka,T., Yamamoto,M., Kato,R., Fukuyama,K., Inoue,Y. and Kuramitsu,S. (2000) Crystal structure of a repair enzyme of oxidatively damaged DNA, MutM (Fpg), from an extreme thermophile, *Thermus thermophilus* HB8. *EMBO J.*, **19**, 3857–3869.
56. Perlow-Poehnelt,R.A., Zharkov,D.O., Grollman,A.P. and Broyde,S. (2004) Substrate discrimination by formamidopyrimidine-DNA glycosylase: distinguishing interactions within the active site. *Biochemistry*, **43**, 16092–16105.
57. Hammes,G.G. (2002) Multiple conformational changes in enzyme catalysis. *Biochemistry*, **41**, 8221–8228.